Numerical assessment of a subglacial lake at Svalbard, Spitzbergen

D. Mansutti*,
Istituto per le Applicazioni del Calcolo 'M. Picone' (C.N.R.),
Via dei Taurini,19, 00186 Rome, Italy

E. Bucchignani,
Centro Italiano Ricerche Aerospaziali,
Via Maiorise, 81043 Capua, Caserta, Italy

P. Glowacki
Institute of Geophysics, Polish Academy of Sciences,
ul. Księcia Janusza 64, 01-452 Warsaw, Poland

The likelihood of a subglacial lake beneath Amundsenisen Plateau at Southern Spitzbergen, Svalbard, pointed out by the flat signal within the Ground Penetrating Radar (GPR) remote survey of the area, is justified, here, via numerical simulation.
This investigation has been developed under the assumption that the icefield thickness does not change on average, as it is confirmed by recently published physical measurements taken over the past forty years. As consequence, we have considered admissible to assume the temperature and density in-depth profiles, snow and firn layers included, to be stationary. The upper icefield surface and the rocky bed surface are known in detail.
By adopting a mathematical numerical model, presented on a recent issue of this journal, based on an unsteady Stokes formulation of the ice flow and a Large Eddy Simulation formulation of the lake water flow, first, we compare two different descriptions of ice water content, in the form of a steady depth dependent function and as solution to the mass transport equation, accounting for local strain heating effect. The last approach, finally selected, leads to 13% improvement of the numerical value of the ice top surface velocity vs. measured one. Furthermore a reduced form of the basal shear stress and normal stress, by making easier the convergence of the iterative solution procedure, allows to obtain physically consistent numerical ice sliding velocity values at the rocky bottom, quite improved in comparison to previous numerical results. After 20000 *d* (physical time), although the maximum value of water temperature keeps rather low, the numerical simulation shows that metastability is overcome on more than half of the conjectured basin, with a progressive trend in time in support to the subglacial lake existence. By that time, the numerical subglacial lake surface converges to the GPR flat signal spot with tolerance equal to the GPR measuring error.
Then numerical simulation results meet quantitatively and qualitatively the fundamental aspects of the conjecture, so that further on-site investigations on the subglacial lake (e.g. drilling operations) appear fully justified.

Keywords: Phase-change, Continuum mechanics, Temperate ice, Subglacial lake, Arctic, Finite volumes.

* Corresponding author: *E-mail address:* d.mansutti@iac.cnr.it

1. Introduction

The study of the environment related to subglacial lakes is worth both for their peculiar physical and chemical characteristics, presumably tracing back to past geological periods, and for its similarities with the icy crust of several satellites of the solar system (e.g. Jupiter' moons) where a sub-surface ocean is conjectured [1], [2]. Subglacial lakes are an established and important component of the basal hydrological system of the Antarctic ice sheet, whereas, in Arctic, only two subglacial lakes have been, so far, clearly identified by airborne radio echo sounding in Greenland [3].

Prior to entering the matter of this paper, it is worth to remind the meaning of few technical terms such as *temperate ice, cold ice* and *firn.* They indicate, respectively, ice at melting temperature, ice at temperature below melting point, and layered ice-water-mushy ice as result of successive snow deposition, compression, melting due to local strain heating and regelation events. Temperate ice consists of a mixture of water and ice and it is characterized by the physical quantity called *water content*, involved in the mathematical modelling. An upper layer of snow and firn usually covers the accumulation icefields. An *ice divide* is a virtual vertical plane within an icefield where ice flows down and departs away from both sides.

Ground-based radio-echo sounding records of the Amundsenisen Plateau, South-Spitzbergen, Svalbard, have revealed several 'flat' bedrock sections, the largest one being 450 *m* long [4]. Amundsenisen Plateau is an accumulation icefield, 80 km^2 in area, with the thickest firn-ice cover of the archipelago (631 m maximum thickness), occupying a large depression surrounded by mountain ridges, controlled by geological structure, with three outlet channels. From thermal viewpoint Amundsenisen Plateau is a temperate icefield. By reflecting properties and estimates of the hydraulic potential field, the 'flat' bed sections might be interpreted as from near-bottom water bodies, indeed very similar to radar reflection from subglacial lakes. Actually their collocation supports this conjecture because they are found beneath a flowing ice stream and/or in the proximity of an ice divide [5], where water drainage occurs. The interest of identifying the nature of the 'flat' bed rock sections is not only geographical but also paleobiological, as deposits from the period before glaciation of Europe and Scandinavia might be collected in the corresponding basins. Then, we focus on the largest 'flat' bed section and, here, aim at the assessment of the conjecture of the existence of a subglacial lake.

In a previous paper [6], we have approached this problem by proposing a mathematical numerical model and a checking algorithm which adopt the assumption that space average ice elevation temporal variation may be assumed negligible. Fundamental support to this choice comes from data collected via airborne laser altimetry by NASA in the time interval 1990-2005 (personal communication by J. Jania), and from observation data on the long-term elevation changes over the past 40 years (Nuth et al., 2010 [7]). From physical viewpoint the stationarity of the icefield top surface elevation has the important consequence that, in time average, the ice loss from icefield outlets and water drainage at the rocky bottom equals the new accumulated ice mass at the top. This fact justifies crucial modeling simplifications. In [6], by sensitivity numerical testing, conclusion reached was that the model must include the description of the local effect of the water content of ice on ice dynamics and the thermal effect of the snow and firn layers on top of the icefield. In this work we discuss the simulation results computed by upgrading the model with the transport equation for water content including strain heating effect. It has to be noticed, here, that a simplified formulation of the ice sliding condition at the rocky bed, allowing straightforward convergence of the numerical solution iterations, has yield an improved numerical estimate of the local ice flow. Furthermore a new, physically consistent, ice driven subglacial water flow has been adopted to initialize the numerical study of the lake water evolution. The likelihood of the lake is verified by comparison of the numerical results with target measured quantities.

The structure of the paper is the following: in Section 2, the mathematical model of the dynamics and thermodynamics of the icefield and the subglacial water is sketched with the introduced updates; in Section 3, the numerical results are described and commented, and in Section 4, conclusions are drawn.

2. Model equations

An orthogonal Cartesian reference system *R(O; x,y,z)* is fixed with *(z),* vertical axis and origin, O, at sea level.

2.1 Icefield equations

Ice is modelled as an incompressible isotropic non-linearly viscous fluid, being characterized by the following effective viscosity μ_i according to the Glen's law:

$$\mu_i = 2^{-(1+n)/2n} A^{-1/n} \left\{ tr\left(D^2\right) \right\}^{1-n/2n} \tag{1}$$

with $n=3$, *tr,* the trace operator, $D = \frac{1}{2}\left[\nabla\vec{u} + (\nabla\vec{u})^T\right]$, the rate of strain tensor, $\vec{u}$, the ice velocity vector and *A,* the so called *flow rate function* which is detailed in the next subsection. For the characteristic slowness of ice flow, the Stokes form of the equations for momentum and mass conservation laws is adopted

$$\begin{aligned} &\rho_i \frac{\partial \vec{u}}{\partial t} = -\nabla p + \nabla\cdot\left\{\mu_i\left[\nabla\vec{u} + (\nabla\vec{u})^T\right]\right\} + \rho_i\vec{g} \\ &\nabla\cdot\vec{u} = 0, \end{aligned} \tag{2}$$

where *p,* is the pressure field, ρ_i, the ice density, amounting to $\rho_i = 910 \ \frac{kg}{m^3}$, and $\vec{g}$, the gravitational acceleration.
In the considered case with temperate ice, it is not necessary to solve the energy conservation equation, as the temperature is a priori known and equal to the pressure melting temperature estimated by the Clausius- Clapeyron law: $T_m(p) = T_0 - \beta p$, with $\beta = 9.7456\cdot 10^{-8}\ K\ Pa^{-1}$ and $T_0 = 273.15\ K$.

2.1.1 Water content and flow rate function

We have considered the water content correlation and the related flow rate functions proposed by Breuer et al. [8], based on characteristic data typical of King George Island temperate ice cap (South Shetland Island, Antarctica). For the physical similarities of that icefield with our study case, we report those functions below.
Called $z_{min}(x, y)$ and $z_{max}(x, y)$ respectively the value of the z coordinate of bottom and top icefield surface at the abscissa x, the estimate of the water content *W* as a function of $z_{max}(x, y)$ and of the normalized thickness z_n, $z_n=(z - z_{min}(x, y))/(z_{max}(x, y)- z_{min}(x, y))$, results:

$$W(z_n, z_{\max}) = \begin{cases} 0.6\cdot\exp(1-z_n)^4, & \text{at } z_{\max}(x,y) < 400m \\ \dfrac{675m - z_{\max}(x)}{675m - 400m}\cdot 0.6\cdot\exp(1-z_n)^4, & \text{at } 400m \le z_{\max}(x,y) < 675m \\ 0, & \text{at } z_{\max}(x,y) \ge 675m. \end{cases} \tag{3}$$

For the sake of clarity, in the following function, temperature is measured in °C and transformed into $T^*=T + \beta p$, in order to overcome the dependency of the melting point on pressure; then, assigned

$$A(T^*,W)=\begin{cases}(1+1.81\cdot W) & \text{at } T^*=0°C\\ \left[1.01+\left(1-\dfrac{W}{0.6\exp(1)}\right)\cdot 0.126\cdot T^*\right]\cdot & \\ \left[1+\left(1+\dfrac{T^*}{2}\right)\cdot 1.8125\cdot W\right] & \text{at } -2°C\le T^*\le 0°C\\ \left(0.925+0.084\cdot T^*\right) & \text{at } -5°C\le T^*\le -2°C\\ \left(0.855+0.07\cdot T^*\right) & \text{at } -8°C\le T^*\le -5°C\end{cases} \tag{4}$$

the proposed flow rate function has the following expression:

$$A=A(T^*,W)\cdot 3.171\cdot 10^{-24}\,Pa^{-3}s^{-1}. \tag{4'}$$

The evaluations at lower ranges of temperature in (4) hold within firn and snow layers, upon the temperate core of the glacier.
Following Hutter [9], [10] and Greve [11], [12], a more general description of the local water release is based on the mass transport equation with a source term, accounting for strain heating effects; in this formulation W meets the following equation:

$$\rho_i\vec{u}\cdot\nabla W=\nu\nabla^2 W+M,\quad \text{with}\quad M=4\mu_i tr(D^2)L^{-1} \tag{5}$$

where ν is the water diffusivity and M is the water production source term with $L=335\cdot 10^3\,JKg^{-1}$, being the latent heat of ice. In many cases ν is assumed to be negligible or is introduced just in support to the numerical stability; actually, only one boundary condition in each coordinate direction is physically justified. Since we adopt $\nu=0.01$, an additional formal boundary condition is to be included, as we shall see later.
Let us stress that the formulation (5) overcomes the limitation of Breuer et al.'s one, that includes only the effect of relative sliding of superimposed ice layers by using the depth dependence of W, and takes into account strain heating induced by any kind of ice deformation.
As reminded in Section 1., in the considered problem, balance between water loss (due to drainage at bottom rocks and ice flow at icefield outlets) and new accumulated ice at the top is assumed, for this reason no internal drainage effect is accounted for in equation (5). In addition Paterson [13] observes that intergranular permeability of temperate ice is extremely low.
In the present application, temperate ice is covered with a coat of snow and firn, 25 m thick, at lower temperature, $273.13\,K\ge T\ge 265.15\,K$. This one has a layered structure and its temperature profile is known from literature ([14], [6]): in time average and from top downwards, temperature increases from 265.15 K (average external temperature) to 271.15 K within the initial 2.5 m thick layer (snow), then it decreases to 268.35 K within the following 2 m and increases definitely to melting temperature by approaching 12 m in depth. So we have chosen to obtain the water content estimate within such an upper layer via Breuer's formula (3) and to upgrade the modelling by combining it with the solution to the equation (5) for the lower temperate ice core. The flow rate function expression is kept unchanged.
The boundary conditions, appropriate within this pattern and completing equation (5), result:

$$\frac{\partial W}{\partial n_b}=0,\ \text{at the rocky bottom,} \tag{5'}$$

$$\frac{\partial W}{\partial x}=0,\ \text{at left and right vertical icefield boundaries,} \tag{5''}$$

$$W=W(z_n,z_{\max}),\ \text{at the firn/temperate ice interface,} \tag{5'''}$$

where the last assignment is evaluated via formula (3).

2.1.2 Boundary conditions and ice sliding on bedrock

Boundary conditions corresponding to the characteristics of the physical system are required in order to determine the numerical solution to the system (2). In the considered test case, the following conditions are imposed at the boundaries of the icefield domain:

$\tau \cdot \hat{n}_s = 0$ with τ, ice stress tensor and $\hat{n}_s$, normal unitary vector (*air/ice interface*) (2')

$$\frac{\partial \vec{u}}{\partial n} = 0 \qquad (outflow) \qquad (2'')$$

$$u=0,\ \frac{\partial v}{\partial n} = 0. \qquad (ice\ divide) \qquad (2''')$$

Details can be found in [6]. At the icefield/rocky bottom boundary condition, a simplified form of the boundary condition is adopted.

Let us recall the phenomenological Weertman-type sliding law, quantifying the basal sliding velocity of ice, $\vec{v}_b$, when basal temperature is at pressure melting point:

being $\hat{t}_b$ and $\hat{n}_b$, the bottom surface tangential and normal outward (pointing to the rocky basement) unitary vectors respectively, the condition reads

$$\vec{u} = \vec{v}_b = C_b \frac{\tau_b^p}{N_b^q} \hat{t}_b \qquad (ice/bedrock) \qquad (2^{iv})$$

where $\tau \cdot \hat{n}_b = \tau_b \hat{t}_b + N_b \hat{n}_b$ is the stress undergone by the icefield at the rocky bottom (τ_b, basal shear stress, and N_b, normal stress), p and q are integer exponents modulated according to the specific natural set-up ($(p,q)=(3,1)$ or $(3,2)$ for sliding on hard rock and $(1,0)$ for sliding on soft, deformable bottom) and C_b is a constant to be tuned according to available data.

We have experienced in [6] the effect on numerical solving of the occurrence in $(2'^{v})$ of the cumbersome expression of the ice stress tensor, τ, leading to quite heavy iterative procedures. Here we have simplified condition $(2'^{v})$ in order to reach the convergence of the internal iterations more rapidly and, as a matter of fact, in order to obtain a numerical solution with higher precision. This is realized with the Shallow Ice Approximation estimates of N_b and τ_b:

$$N_b = -\,p_{eff} = -[\,\rho_i g(z_s(x,y) - z_b(x,y)) - \rho_w g z_b(x,y)\,], \qquad (2^{v})$$

the *effective pressure* resulting from basal water pressure minus ice overburden pressure, and

$$\tau_b = N_b \cdot \sin\alpha, \qquad (2^{vi})$$

with α the average bottom surface slope. This approach, suggested and adopted also by other authors (e.g. [13], [15], [16]), corresponds to neglect the local contribution of the normal stress deviators τ_{xx}, τ_{yy} and τ_{zz}, as well as the shear stress in the vertical planes, τ_{xy}. This is substantially justified by the predominant role of basal water in governing icefield sliding.

In consideration of the relatively small extension of the conjectured subglacial lake, that does not support the onset of ice recirculation [6], we have extended the validity of condition (2^{iv}) as dynamical boundary condition for ice equations also at the icefield/subglacial lake front.

2.2 Subglacial lake equations and boundary conditions

The model of the hydrodynamics of the conjectured subglacial lake is based on a Large Eddy Simulation approach with constant eddy viscosity and thermal diffusion coefficients as extensively described in [6]. Within an extended Boussinesq approximation, water is assumed incompressible

except for the buoyancy term where the peculiar relation among density, temperature and pressure (equation of state) is taken into account (Chen and Millero, 1986 [17]). The momentum, mass and energy conservation equations follow:

$$\begin{aligned}
&\frac{\partial \vec{u}}{\partial t} + \nabla\cdot\, \vec{u}\vec{u} = -\frac{1}{\rho_0}\nabla p + \nabla\cdot\left(\vec{A}^M \nabla\vec{u}\right) + \frac{\rho_w}{\rho_0}\vec{g} \\
&\nabla\cdot\, \vec{u} = 0 \\
&\frac{\partial T}{\partial t} + (\vec{u}\cdot\,\nabla)T = \nabla\cdot\left(\vec{A}^H \nabla T\right)
\end{aligned} \qquad (6)$$

where thermal effects of dissipation have been neglected, the usual meaning of the variables, $\vec{u}$, p and T, holds and, furthermore, ρ_0 and ρ_w are the functions of water density respectively at sea level $(p = 0)$ and at pressure value p.

For reasons that will be explained in the next section, the system icefield-lake is approached in a two-dimensional domain (see Section 3), accordingly we provide the remaining details of the model. $\vec{A}^M = (A_{\mathrm{h}}^{\mathrm{M}}, A_{\mathrm{v}}^{\mathrm{M}})$ and $\vec{A}^H = (A_{\mathrm{h}}^{\mathrm{H}}, A_{\mathrm{v}}^{\mathrm{H}})$ are the vectors of eddy viscosity and thermal diffusion coefficients that, accounting for the results of the numerical tests developed in [6], have been assigned to $\vec{A}^M = (5,\, 10^{-4})$ and $\vec{A}^H = (9.09,\, 10^{-5})$.

The partial differential system is completed with the following boundary conditions at the bedrock:

$$\begin{aligned}
&\frac{\partial u_t}{\partial n} = 0 \\
&u_n = 0, \\
&-\left(A_h^H \frac{\partial T}{\partial x} n_{b,x} + A_v^H \frac{\partial T}{\partial z} n_{b,z}\right) = \frac{1}{\rho_w c_w} q_{geo}
\end{aligned} \qquad (7')$$

being u_t and u_n, the tangential and normal velocity components, c_w, the subglacial water heat capacity, and q_{geo}, the geothermal heat flux, amounting to $37.5 mW/m^2$ in the considered region [6].

Furthermore jump conditions between the phases, one per each conservation equation, have to be imposed at the icefield/subglacial lake interface. In particular the thermal jump condition (*Stefan condition*) (8) regulates the evolution of the interface, most critical aspect here:

$$Lu_n = -c_w\left(A_h^H \frac{\partial T^w}{\partial x} n_x + A_v^H \frac{\partial T^w}{\partial z} n_z\right) + \frac{k_i}{\rho_0}\frac{\partial}{\partial n}\left(T_m(p)\right), \qquad (8)$$

with $L = 333.5\ 10^3\ J/kg$, the latent heat of fusion of ice, and k_i, the ice thermal diffusivity.

For the explicit form of the other jump conditions we refer the reader to [6].

3. Numerical test

The detection of the space domain within the Amundsenisen icefield, most suitable to proposed investigation, is part of the work in [6] and was accomplished by running the three-dimensional computational code Elmer/Ice (open source *http://www.csc.fi/elmer/,* only ice dynamics and thermo-dynamics [18]) on the space geometry delimited by the measured bottom and top surfaces of the plateau, up to reach a steady regime. In Figure 1 the computed ice velocity field at the icefield bottom is shown. We notice that it is appears to be split into two parts by an ideal diagonal line (projection of an ice divide to the bedrock) from which ice flow departs either from below and from above. Furthermore, in the upper half part of the icefield, where it has been detected the flat signal from Ground Penetrating Radar [4] of the conjectured subglacial lake – reference geographical coordinates (511 000, 8 582 000) -, we notice that flow is parallel that is substantially two-

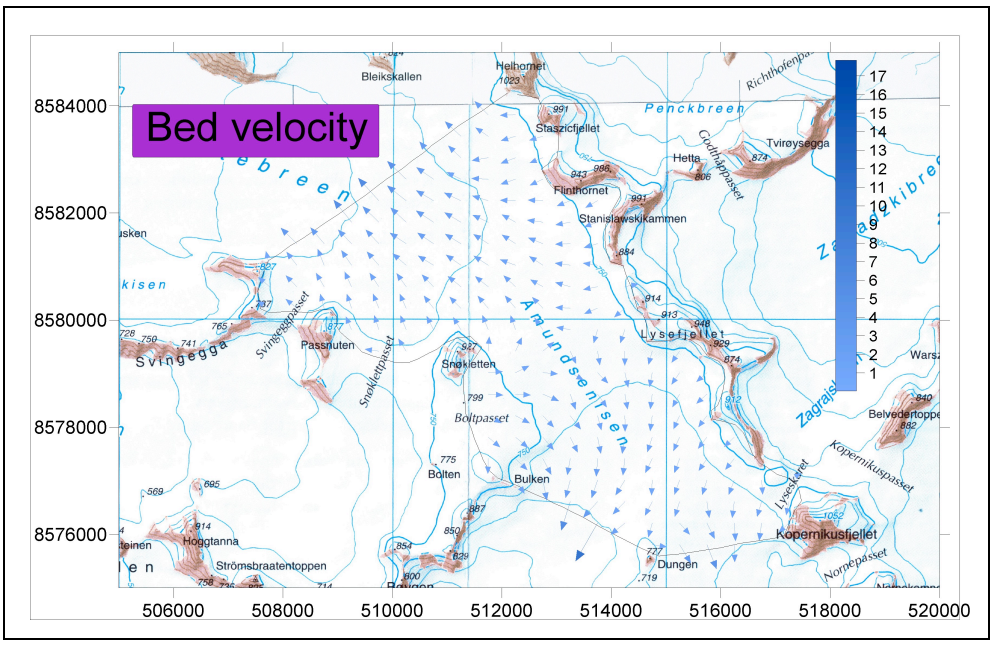

Figure 1: Icefield velocity field at the bottom surface computed with the Elmer/Ice code (*m/yr*) .

dimensional. Definitely the relatively small extension of the flat signal spot ([6], [19]) allows to approach the study case in a two-dimensional domain that is selected by intersecting the icefield with a vertical plane parallel to the ice flow field across the spot. We fix the *(x)*-axis along the direction of the ice flow.

The hypothesis of a subglacial water channel network in Antarctica has fostered, in polar applications, the use of reformulations of the model in terms of enthalpy, based on a fixed space grid [20]. However, in present case involving the identification of the icefield/subglacial lake interface, the classical multi-physics domain decomposition approach, described in Section 2, results more straightforward although repeated recomputation of variables on time changing discrete space meshes contributes significantly to the procedure computational cost .

As extensively explained in [6], the numerical solution of the partial differential system is based on a finite volume method. In Figure 2 the space domain of the icefield and of the conjectured lake with the related prototypical finite volumes grids are displayed. For the choice of the depth of the lake, in [6] the experimentation has been reported; furthermore, it is shown that larger depth enhances the processes leading to lake formation and stability.

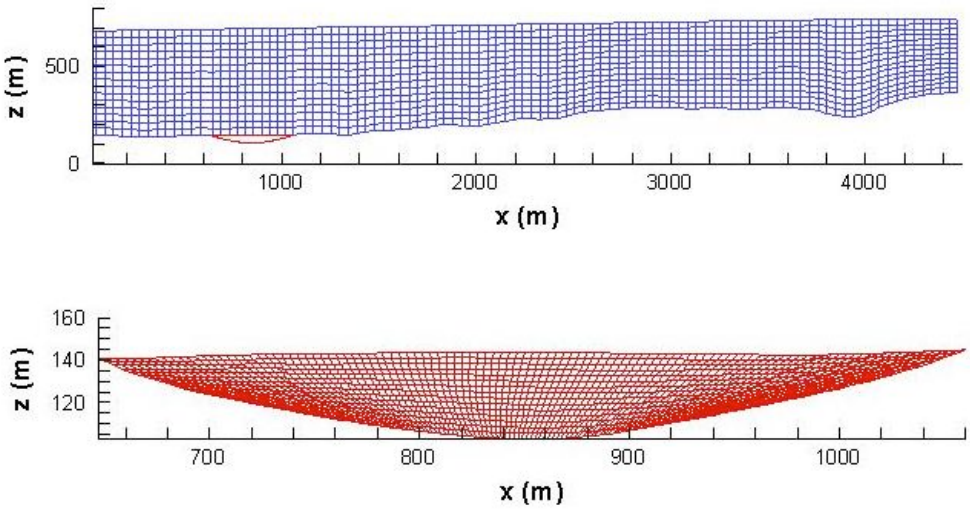

Figure 2: Icefield (upper) and subglacial lake (lower) space domains and prototypical finite volume grids.

A double step nested time integration procedure, which takes into account the different ice and water time scales, is adopted. Time discretization has been done with a second order implicit scheme with time steps granting satisfactory accuracy (versus convergence) that is $\Delta t_i = 0.5\ day$ with space mesh size 301×46 and $\Delta t_w = 7.2\ min$ with space mesh size 113×31, respectively for the icefield and for the subglacial lake. In [6] the results of the refinement space mesh analysis for the icefield and the choice made in either case are discussed.
A linearization technique preserving good coupling among the equations and the Bi-CGSTAB algorithm for the solution of the linear systems are adopted in each phase. The phase front is updated by solving the equation of the Stefan condition within the icefield time integration cycle (that, obviously, includes the lake water time integration cycle); afterwards, the icefield and subglacial lake discretized domains are redrawn by a front-tracking technique and variables recomputed on the new mesh points by linear interpolation (or extrapolation, where necessary).

3.1 Initial condition

The initial condition required to complete the unsteady partial differential model adopted is built up as follows.
The initial ice flow has been extracted from the mentioned Elmer/Ice numerical regime solution. For initialization of the lake variables, we aimed at keeping as close as possible to values suitable to the ice state, as if the lake water were still in metastable state, avoiding unnecessary artificial numerical support to the conjecture of the existence of the subglacial lake. Then the velocity field, under the icefield driving action at the phase front, is obtained via linear extrapolation of the ice flow in order to represent that lake water motion would arise smoothly from the icefield motion. Moreover a temperature linear profile is adopted with the limitation

$$T_m(p) < T(t_0,x,z) < T_m^{\ ph}$$

being T_m^{ph}, the pressure melting temperature at the icefield/subglacial lake interface. As $T_m^{ph} \approx 272.658\ K$ and, at the deepest point of the conjectured lake bottom, $T_m(p_{\max}) = 272.62\ K$, such a profile results weakly decreasing (from top to bottom) and indeed very close to pressure melting temperature values: we call this transient state 'liquid ice'.
As initial values are very critical versus the aim of this work, the validation of the conjecture of the subglacial lake, we characterize the choice made above with a straightforward thermo-dynamical argument considering the heat of fusion of the ice mass, that we picture originally placed in the conjectured bedrock depression, and the time required to the phase change process to transform ice into water thus forming the lake within the described general physical set-up.
An approximate estimate of the amount of heat available for melting the ice in the lake cavity can be obtained with the geothermal heat flux from the lake bottom surface reduced by the lake top surface; hereafter, an explanation follows. As authors explained in [6] with the support of data in [4] and [7], at Amundsenisen Plateau ice thickness may be considered (in average) constant in time which implies that, being an accumulation area, the new overlaying snow (after transforming into firn and ice) equals the melt water at bottom, drained through the rocks. Then, regardless the lake does exist or does not, it seems reasonable to suppose that the drained water amounts about the same along the whole icefield bottom surface, so that, also in correspondence of the lake, it can be approximated with the water released by the portion of icefield above it as if it were in contact with the soil, absorbing the geothermal heat from an area equal to the lake top surface. In the considered case, lake top and bottom lengths are respectively $S_l \approx 420\ m$ and $S_b = 437\ m$, then, heat income left for lake water release would amount to

$$\Delta Q_{geo} = (S_b - S_l) \cdot \mathrm{q_{geo}} = (437\ m - 420\ m) \cdot 37.5\ mW/m^2 = 6.375 \cdot 10^{-1} J/(s\ m)$$

(as the problem formulation is two-dimensional, the estimate of ΔQ_{geo} is computed per section thickness unit).
Furthermore the heat of fusion of the ice in the conjectured bedrock depression can be calculated from $Q_m = L \cdot \rho_i \cdot V_l$, with L, latent heat, ρ_i, ice density and V_l, the considered volume section of the

lake, roughly estimated to be $V_l = S_l\, d_l/2 = 10{,}080\ m^2$ per section thickness unit, being $d_l = 48\ m$ lake maximum depth.
It results $Q_m = 333.5 \cdot 10^3 \cdot 917 \cdot 10080 = 3.083 \cdot 10^{12} J$ per section thickness unit.
Accordingly it comes that the time required for ice mass in the bedrock depression to melt can be estimated with

$$\Delta t_m = Q_m \Big/ \Delta Q_{geo} = 3.083 \cdot 10^{12} \Big/ 6.375 \cdot 10^{-1} = 0.4836 \cdot 10^{13}\, s = 153{,}000\ yr.$$

We stress that above argument has been developed with fixed values of q_{geo}, L and ρ_i and unchanged local bedrock morphology for this reason it represents a qualitative physical justification to the selected initial values, becoming quantitatively sound provided that it is possible to assume that, during a past time interval of such a order, these parameters do not vary significantly. External conditions (e.g. air temperature) are not directly involved.

3.2 Selection of the water content formulation

The first numerical test has been finalized to check if the simpler representation of water content (3) is sufficient to describe the complexity of the icefield state or if equation (5), more complete from physical viewpoint, is necessary. At this purpose we compare the iso-surfaces of W obtained with the first formulation, shown in Figure 3, with the corresponding ones, displayed in Figure 4, computed at time $t = 2000$ *d(ays)* with the second formulation. We see that differences are quite evident and, even before an evaluation of the validity of the results, as equation (5) is an upgrade of the model, they point out that its adoption is necessary: although both plots exhibit that water is mostly present within ice adjacent to the bedrock, Figure 4 shows that water particles form especially at bedrock undulations where ice flow changes direction and, consequently, generates viscous strain heating; from there, they are transported via diffusion and by the ice flow leading to such an horizontal

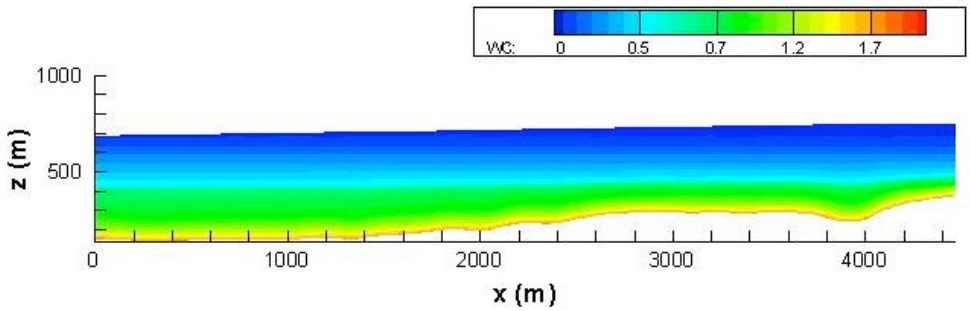

Figure 3: Icefield: *w*ater content iso-surfaces as they appear according to the (steady) Breuer et al.'s correlation function (3).

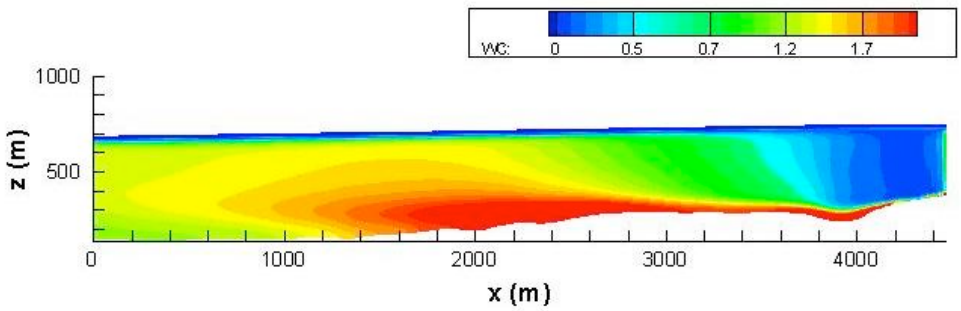

Figure 4: Icefield: water content iso-surfaces at *t=2000 d* computed by numerical simulation with equation (5).

flame shape of the *W* iso-surfaces. In Figure 5 the two vertical profiles of water content at the abscissa *x = 2000 m* are compared. The natural reason for the evident water content decrease with altitude, in common to both representations, is the increase of melting temperature due to the reduction of hydrostatic pressure. For the upgraded model such a decrease has a strong nonlinear character: we see an abrupt change at *z =300 m*, where ice flow undergoes no longer the effect of the rocky bottom, and at *z = 650 m*, where water content starts to decrease faster for the vicinity of snow and firn and of the icefield/air interface where its value is null because of the external temperature below melting point. The null normal derivative imposed as boundary condition to equation (5) is responsible for the smooth step-shaped curve of *W* at the bedrock.

From [4] we know the (measured) value of the top surface ice velocity at the outlet above the conjectured subglacial lake that amounts to *26.35 m/yr*. We have adopted this value as target of our

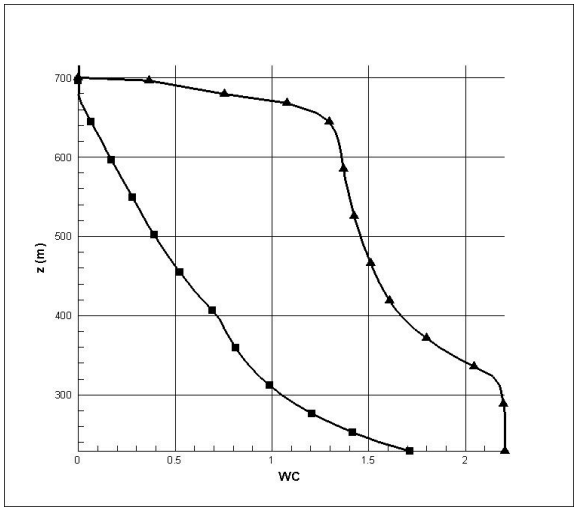

Figure 5: Icefield: water content profiles at time *t = 2000 d* at *x = 2000 m,* computed via correlation (3) - squares – and equation (5) – triangles .

numerical simulation (measuring error and time variability are assumed negligible).

In Figure 6 the outlet vertical profiles of the ice horizontal velocity are compared in the two cases: it is well visible that the result obtained with the use of equation (5), *U = 30 m/yr,* is more accurate than the one computed by adopting correlation (3), *U = 33.4 m/yr*, with an improvement of accuracy of 13% versus the target value. This trend is justified by the fact that the longitudinally uniform distribution of water particles along the bottom profile, in Figure 3, supports sliding better than the non-linearly decreasing distribution (see from abscissa x $\approx$ 1700 m backward to the outlet), in Figure 4, that has an overall slowing down effect dispite water content attains locally larger values.

We have monitored ice water content evolution till *t = 16000 d* and noticed that its spatial distribution and value remain essentially unchanged. It is worth to remind that, in the present model, strain heating is enabled to induce just water formation and not temperature increase, according to the real natural set up with temperature at pressure melting point along with the persistence of temperate ice. The existence of a steady water content distribution implies that either the whole amount of developed strain heating is used for the preservation of such a quantity of water and the increase of water particles within ice texture decreases local strain heating production.

3.3 Validation of the conjecture of a subglacial lake

The rationale of the validation procedure adopted is to verify if the numerical simulation of the

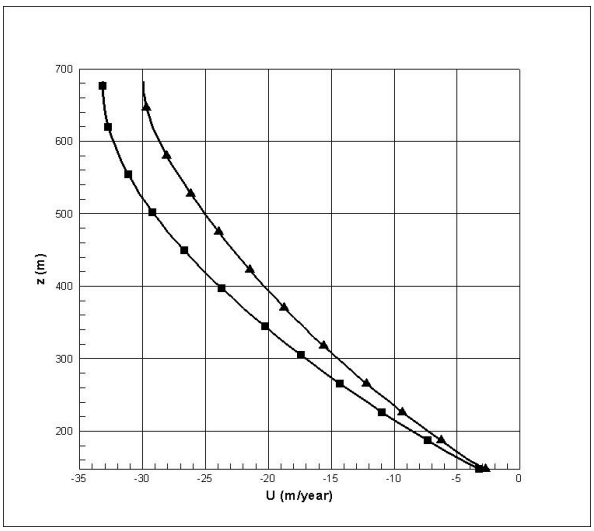

Figure 6: Icefield: horizontal velocity profile along the outlet at $t = 2000\ d$ computed by adopting correlation (3) - squares – and equation (5) – triangles.

icefield including a conjectured bedrock depression – lake cavity – evolves with the formation of a lake consistently with the real natural set-up.

In the vicinity of the icefield/lake water front, the description of the water content of ice influences also lake water dynamics and heat transfer through ice dynamics. So, within this experimentation, the choice of the advanced model (5) might be critical. Similar impact has also the description of the ice sliding-on-bedrock velocity that has been, here, obtained with the adoption of the simplified form of the basal shear stress in (2^{vi}). Let us notice that the simplification has allowed to assign in (2^{vi}) the constant $C_b = 10^{-6}$ and the parametrical exponents $(p,q) = (3,1)$, the last ones according to the indications in [13] for the case of sliding on hard beds. In [6], just the choice $(p,q) = (1,1)$ – preferred for soft beds - was possible.

At bedrock the value of the ice horizontal velocity component at the outlet is detectable in Figure 6 and amounts to $U = 2.6\ m/yr$, consistently with the physical process (see Figure 1). As a matter of fact, in [6], full basal shear stress formula yield only negligible – unphysical - sliding velocity due to its extreme complexity which made difficult the convergence of linear system iterations.

In Figure 7 and in Figure 8 the iso-surfaces of the ice horizontal velocity and of the subglacial lake water temperature with particle tracks are, respectively, shown at time $t = 16000\ d$, when the simulation seemed to have reached a steady state: ice flows at increasing velocity from the ice divide (at right) towards the outlet (at left), lake water circulates in a convection cell consistent with the driving action of the icefield as by physical anticipation and about 40% of the basin is occupied by

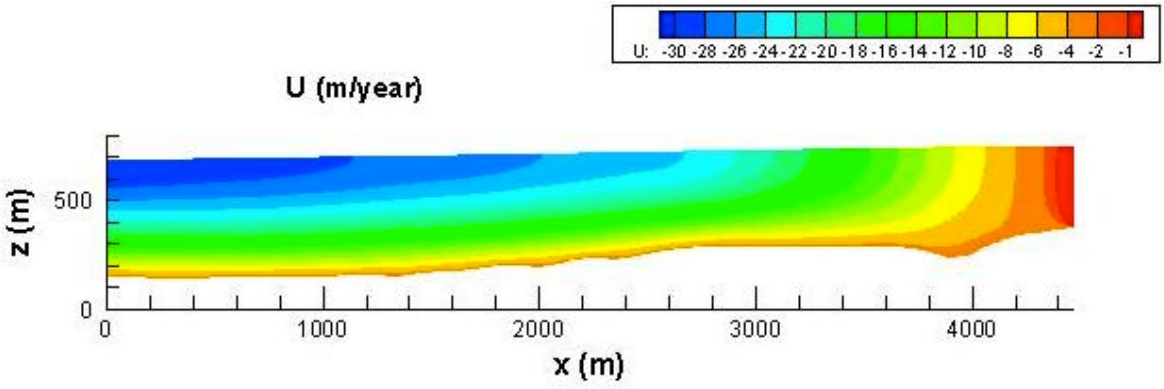

Figure 7: Icefield: horizontal velocity iso-surfaces at $t = 16\ 000\ d$.

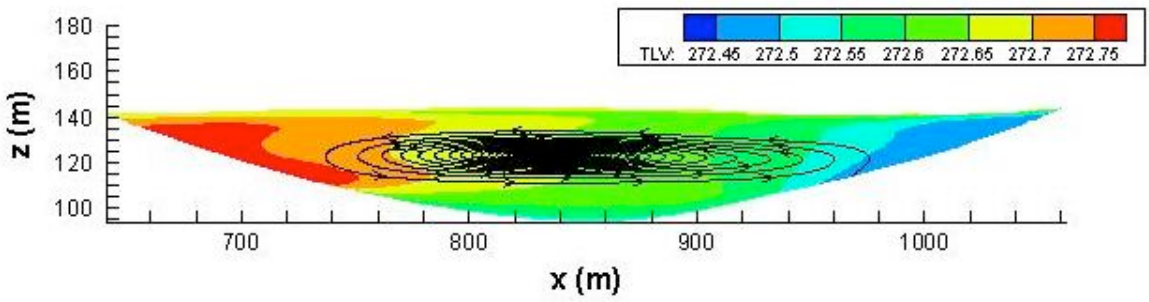

Figure 8: Subglacial lake: temperature iso-surfaces and particle tracks at t = 16 000 d.

water at temperature $T(t,x,z) > T_m(p)$. Meanwhile the top surface ice velocity at the outlet keeps less or equal *30 m/yr*, as reported already at *t = 2000 d* in Figure 6, which implies that icefield bottom shape modification due to phase change (see Stefan condition (8)), does not affect significantly the icefield dynamics.

The plot of the ice/subglacial water interface at several time instants, shown in Fig. 9, exhibits profiles converging to the last one, pointing out the achievement of local thermo-dynamical equilibrium (see Stefan condition (8)). It is clearly visible that, along with the time evolution, ice melts (and ice/water interface moves forward towards the icefield) at the left side of the basin where heat is transported by the convection cell, whereas, at right, part of the initial 'liquid' mass overcomes metastability transforming into ice (ice/water interface moves backward from the icefield). The last interface profile results modified versus initial one (that was rebuilt from collected GPR signal) with maximum change of *40 cm* at left and *2 m* at right.

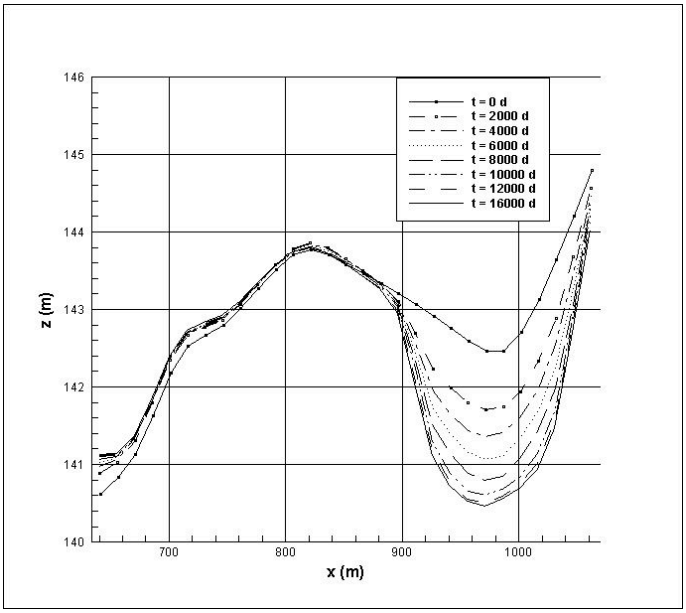

Figure 9: Evolution of the ice/subglacial water interface.

In fact, in the water below the upper thermal boundary layer, transfer of geothermal heat from the rocky bottom to the lake water bulk goes on till a possible thermodynamical equilibrium is reached in the system, where heat is redistributed within the lake by convection-diffusion meanwhile icefield rheology and temperature profiles are kept fixed to the observed status. However it is very difficult to assess the existence of a steady configuration with absolute confidence, due to the intrinsic slowness of the overall process and the heaviness of the numerical computation. So we have carried on the numerical simulation for a further time slot of *4000 d* and compared several configurations obtained

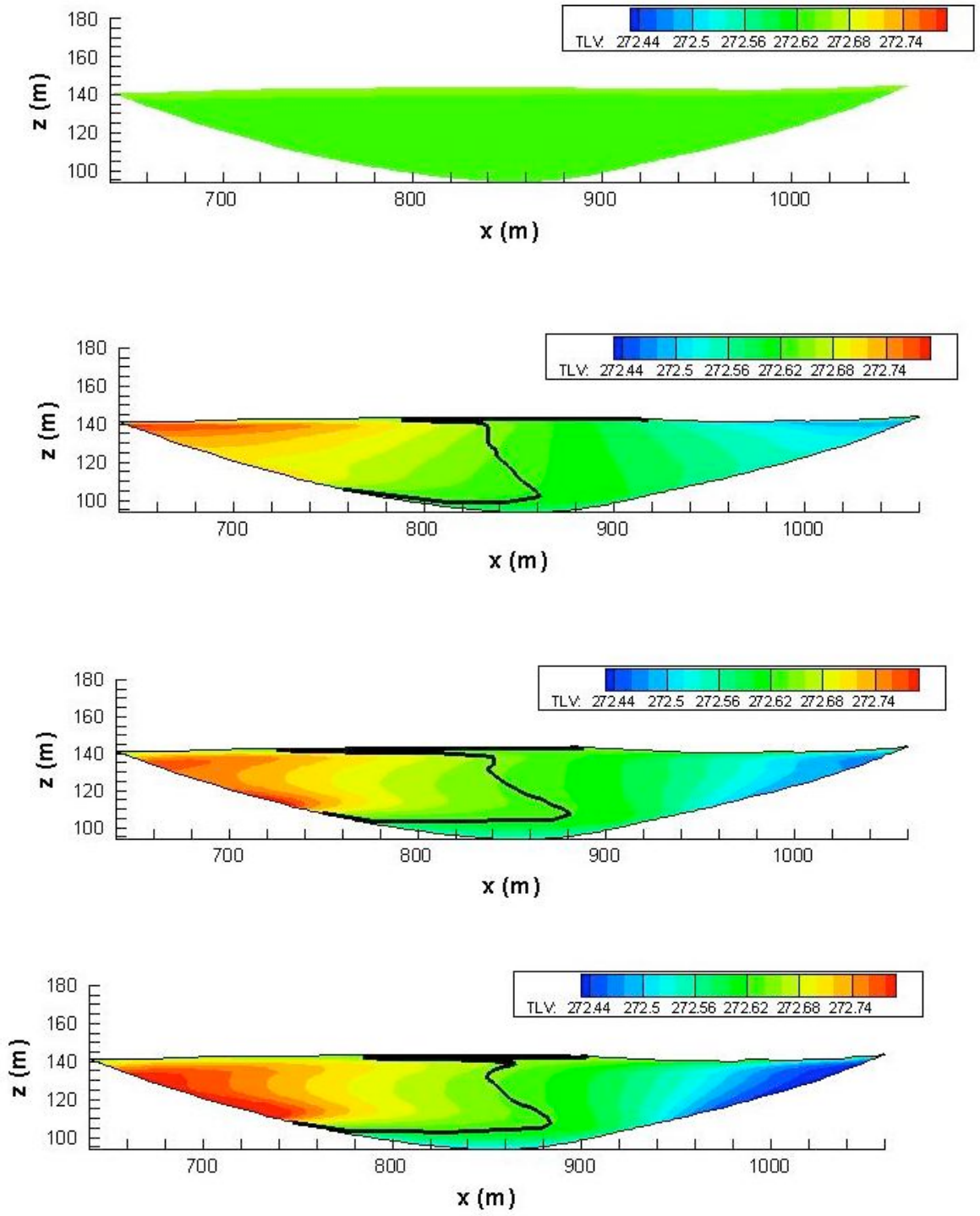

Figure 10: Subglacial lake: isothermal surfaces and metastability line (in black) with stably melt region at its left at time *t = 0, 4000, 12000* and *20000 d* (from top).

in order to bring out the trend of the process and to reach a conclusion about the existence of the subglacial lake.

In Figure 10 we show numerical results at times *t =0, 4000, 12000* and *20000 d.* Initially ice occupying the bedrock depression – top picture -, being in the so called 'liquid ice' transient state (see Section 3.1), is supposed to have already structure bonds weakened by geothermal heat inflow to such a point that the constitutive equation of a liquid might appropriately describe its dynamical evolution. In the time following the established fluid structure has allowed the onset of a convection cell that contributes significantly to the geothermal heat transfer into the bulk, leading to the temperature iso-

surfaces plot at time $t = 4000\ d$. The metastability line (that is drawn in black) separates the stably formed water from the transient 'liquid ice' state. From the two pictures below, at times $t = 12000\ d$ and $t = 20000\ d$, it is visible that the region occupied by stable water increases slowly with time, and its local temperature too.
This trend is expected to go on and eventually, the metastability line to move to the right side, and converge to a curve that adjusts the lake bottom profile towards a cavity filled of water with shape compatible, within the mathematical model adopted, to the fixed boundary conditions (7'). The cold region at right side, whose temperature is two degrees below melting point, is filled with 'liquid ice' drifted back to ice state.

4. Conclusions

A numerical simulation has been developed with the aim to check the validity of the conjecture of a subglacial lake at the Amundsenisen Plateau in South Spitzbergen, Svalbard, in correspondence of a flat signal spot detected within a Ground Penetrating Radar remote survey of that area.
First, we have shown that, if a bedrock depression exists beneath the icefield and climatic and environmental conditions do not change significantly, geothermal heat accumulates within ice in the cavity (see Section 3.1): part of it melts the water drained through the rocks and the exceeding one, ordinarily leading to temperature raising up to melting point, as Amundsenisen icefield is temperate (in metastable state), causes the weakening of the structural ice bonds and, eventually, the phase change. After a time interval, whose duration depends on q_{geo}, L and ρ_i, the whole ice in the cavity will be transformed into water. Then, we have verified by numerical simulation that the evolving dynamics and thermodynamics of the two-phase system, icefield-lake, at present physical conditions, lead to an increase of temperature of the water basin, stating the ultimate departure from metastable state. As commented in Section 3.3, the initial icefield/lake interface undergoes an adjustment by numerical modelling that results well below the measuring error of the Ground Penetrating Radar, providing the corresponding flat signal spot (GPR error generally amounts to $\pm\ 3.5\ m$). This fact implies that numerical subglacial lake surface meats the measured datum.
We can conclude that GPR flat signal spot collected at Amundsenisen is indeed compatible, versus dynamics and thermodynamics implications, with the presence of the subglacial lake. This deduction is enforced by the improved mathematical numerical description of the driving icefield dynamics (with respect to [6]), yielding good matching with physical top surface and bottom surface velocity values. As consequence on-site investigations on the subglacial lake (e.g. drilling operations) appear fully justified.
The numerical simulation, pushed forward possibly to thermo-dynamical equilibrium, would provide the bottom contour of the lake, meant as the line surrounding the water at temperature higher than $T_m(p)$. Here, the simulation has reached $t = 20000\ yr$ (still transient state) and, at that time, the lake bottom contour consists partly of bedrock and partly of meta-stability front.
As already obtained in [6], the cavity depth is a critical quantity. Actually, along the reasoning in Section 3.1, the portion of geothermal heat hold in the cavity, ΔQ_{geo}, depends directly on lake bottom length and, consequently, on lake depth; besides, Δt_m , ice basin melting time or time required for the lake formation, depends inversely on it. So, once the lake will be eventually assessed, its depth might be an element for the development of time involving diagnostic considerations.
It is worth to observe that in our previous work [6], beside the commented differences (see Sections 2.1.1 and 2.1.2) in the ice water content and sliding on bedrock modelling, at initial time we fixed lake water at rest. This lead to a circulation counteracting the icefield driving action, opposite to present numerical result, showing that the time scale of thermal convection induced by geothermal heat is significantly shorter than the one of the icefield driven convection. Present results do not allow to detect if the coherence obtained is due to the improved ice modelling, inducing larger momentum transfer to lake water, or/and to the lake initial flow built by extrapolation of icefield flow. A new simulation starting from lake at rest would clarify this aspect.

A more realistic three-dimensional approach to the presented validation problem should not contradict the conclusions reached. Actually, if we consider a semi-spherical lake cavity and focus on anyone of the vertical sections through the lake axis, we see that icefield driving action and geothermal heat inflow action are not coplanar (on the contrary of the two-dimensional simulation above), then, by combining, they lead to a slower convection flow in that section. As consequence, but in the central vertical section of the lake parallel to the icefield motion, a slower temperature increase along the icefield motion is expected, which should not prevent ice/water phase change and lake formation, although within longer time interval.
A more sophisticated modelling of ice would be obtained with the inclusion of water drainage at the icefield bottom but this one would require historical data series on ice accumulation at top surface, that are very seldom available, in any case not for Amundsenisen Plateau. The drawback of our approach could be to obtain an excess of water within ice texture. However we point out that, in our simulation, ice water content, though slightly exceeding the usual admitted range, does not blow up but it reaches a steady distribution (see Figure 4). We have interpreted this fact as if the whole amount of developed strain heating is used for the preservation of such a quantity of water particles whilst their increase within ice texture decreases local strain heating production.

Acknowledgements – The authors acknowledge the ESF-ERANET PolarClimate Consortium for founding the transnational project SvalGlac – Sensitivity of Svalbard Glaciers to Climate Change (2010-2013); presented results are part of its accomplishments. In particular the national agencies supporting the authors are the following: Piano Nazionale Ricerca Antartide (PNRA) (Mansutti) and Narodowe Centrum Badań i Rozwoju National (NCBiR) (Glowacki). Mansutti wants to thank: Prof. J. Jania (Dept. Geosciencies, University of Silesia) for sharing his knowledge on icefields at Amundsenisen, South-Spitzbergen; Prof. F. J. Navarro (Universidad Politecnica de Madrid) for his expert advice on glaciological issues and Prof. J. Otero (Universidad Politecnica de Madrid) for useful discussion on manuscript content.

References

[1] Carr, M. H., M. J. S. Belton, C. R. Chapman, M. E. Davies, P. Geissler, R. Greenberg, A. S. McEwen, B. R. Tufts, R. Greeley, R. Sullivan, J. W. Head, R. T. Pappalardo, K. P. Klaasen, T. V. Johnson, J. Kaufman, D. Senske, J. Moore, G. Neukum, G. Schubert, J. A. Burns, P. Thomas and J. Veverka, 'Evidence for a subsurface ocean on Europa', *Nature*, **391**, 363-365, 1998.

[2] Mitri, G. and A. P. Showman, 'Convective–conductive transitions and sensitivity of a convecting ice shell to perturbations in heat flux and tidal-heating rate: implications for Europa', *Icarus*, **177**, 447–460, 2005.

[3] Palmer, S. J., J. A. Dowdeswell, P. Christoffersen, D. A. Young, D. D. Blankenship, J. S. Greenbaum, T. Benham, J. Bamber and M. Siegert, 'Greenland subglacial lakes detected by radar', *Geophys. Res. Letters,* **40,** 6154-6159, 2013.

[4] Glowacki, P., A. Glazovsky, Y. Macheret, E. Vasilenko, J. Moore, J. O. Hagen, D. Puczko, M. Grabiec, J. Jania, F.J. Navarro, 'Dynamics and mass budget of Amundsenisen, Svalbard: interpretation of surface elevation and radar data', IUGG 2007, Perugia, 2007.

[5] Ridley, J. K., W. Cudlip and S. W. Laxton, 'Identification of subglacial lakes using ERS-1 radar altimeter', *J. Glaciol*., **39,** 625-634, 1993.

[6] Mansutti, D., E. Bucchignani, J. Otero and P. Glowacki, 'Modelling and numerical sensitivity study on the conjecture of a subglacial lake at Amundsenisen, Svalbard', *Appl. Math. Modelling,* **39,** 4266-4284, doi: 10.1016/j.apm.2014.12.043, 2015.

[7] Nuth, C., G. Moholdt, J. Kohler, J. O. Hagen and A. Ka¨a¨b, 'Svalbard glacier elevation changes and contribution to sea level rise', *Jour. of Geophys Res,* **11**, 1-16, 2010.

[8] Breuer, B., M.A. Lange and N. Blindow, 'Sensitivity studies on model modifications to assess the dynamics of a temperate ice cap, such as that on King George Island, Antarctica', *Journal of Glaciology*, **52** (177), 235-247, 2006.

[9] Hutter, K.,'Dynamics of glaciers and large ice masses', *Annu. Rev. Fluid Mech.,* **14,** 87-130, 1982.

[10] Hutter, K., 'Thermo-mechanically coupled ice-sheet response – cold, polythermal, themperate', *J. Glaciology,* **39**(131), 65-86, 1993.

[11] Greve, R., *Thermomechanisches Verhalten polythermer Eisschielde – Theorie, Analytik, Numerik,* (Phd thesis, Technische Hochschule, Darmstadt), 1995.

[12] Greve, R., 'Application of a polythermal three-dimensional ice sheet model to the Greenland ice sheet: response to steady-state and transient climate scenarios'*, J. of Climate,* **10**(5), 901-918, 1997.

[13] Paterson, W.S.B., *The Physics of Glaciers*, Butterworth-Heinemann, Elsevier Science, 2006.

[14] Zagorodnov V. S., *Ldoobrazovanye i glubnoye stroyenie lednikov* (*Ice formation and inner structure of glaciers*) (Russian), in Glyatsiologiya Spitsbergena (V.M. Kotlyakov, ed.), Nauka, Moskva, 119-147, 1985.

[15] Greve, R. and H. Blatter, *Dynamics of Ice Sheets and Glaciers*, Springer-Verlag Berlin Heidelberg, 2009.

[16] Otero, J., F. J. Navarro, C. Martin, M. L. Cuadrado and M. I. Corcuera, 'A three-dimensional calving model: numerical experiments on Johnsons Glaciers, Livingston Island, Antarctica', *J. Glaciology,* **56** (196), 200-214, 2010.

[17] Chen, C.T. and F.J. Millero, 'Precise thermodynamic properties for natural waters covering only the limnological range', *Limnol. Oceanogr.*, **31**(3), 657-662, 1986.

[18] Gagliardini, O. and 14 others, 'Capabilities and performance of Elmer/Ice, a new-generation ice sheet model', Geosci. Model Dev. **6**, 1299–1318, doi:10.5194/gmd-6-1299-2013, 2013.

[19] Kwok, R., M. Siegert and F. Carsey, 'Ice motion over Lake Vostok,Antarctica: constrains in inferences regarding the accreted ice'*, J. Glaciology,* **46,** 689-694, 2000.

[20] Voller, V. R., C. R. Swaminathan and B. G. Thomas, 'Fixed grid techniques for phase change problems: a review', *Intl. J. for Num. Meth. in Engineering*, **30** (4), 875–898, 1990.